International Journal of Research in Engineering and Science (IJRES)
ISSN (Online): 2320-9364, ISSN (Print): 2320-9356
www.ijres.org Volume 12 Issue 3 ǁ March 2024 ǁ PP. 230-246

Research on flexural performance of composite steel truss without upper chord

CHEN Rongzheng[1], CAO Kaiqiang[2]
[*1]*School of Environment and Architecture, University of Shanghai for Science and Technology, Shanghai 200093, China ;*
[*2]China Railway Fourth Bureau Group Fifth Engineering Co., LTD, 332900, *China ;*
Corresponding Author: 992569200@qq.com

Abstract
The hollow steel truss composite floor without upper chord is a new type of composite floor, which is mainly composed of concrete slab, belly bar, and lower chord bar. The concrete slab is connected with the lower steel member through the stud connector to form the hollow composite floor. At the beginning of this paper, the static loading test of a composite steel truss without upper chord is carried out. According to the relationship between deflection development and load, the whole test process can be divided into three stages: elastic development stage, elastoplastic development stage and failure stage. The load-deflection relationship, strain stress distribution of cross section, stress distribution of belly bar, stress distribution around bending and shear section, crack development and failure mode of composite steel truss without upper chord are analyzed based on test phenomena and test results. The results show that the composite floor has excellent cooperative working ability and good ductility, and the strain distribution along the height is approximately linear at the elastic stage. The stress distribution is more complicated than that of the pure section. The bearing capacity of the composite floor increases with the increase of the number of belly rods. In the whole development stage of the structure, the neutral axis of the hollow section is always located inside the concrete slab. At the end of the elastoplastic stage and near the loading point of the failure stage, cracks develop rapidly. The bare cracks appear at the bottom of the concrete slab in the hollow area of the flexural shear section, and cracks along the distribution area of the belly bar appear at the top of the concrete slab. At this time, most areas of the lower chord bar have entered the full section yield stage.

Keywords: *composite floor； belly bar； lower chord bar.； bearing capacity*

Date of Submission: 05-03-2024 Date of acceptance: 18-03-2024

I. INTRODUCTION

Unwinded hollow steel truss composite floor is a new type of steel-concrete composite floor, which combines two materials of steel and concrete through connecting parts, and combines the advantages of steel structure and concrete structure. Therefore, it has very significant advantages, such as strong bearing capacity, excellent seismic and dynamic performance, small section size of components and convenient construction.

In 1972, AZMI[6] proposed a calculation model of the plastic bending capacity of steel truss-concrete composite beams under full shear connection, excessive shear connection and partial shear connection. The contribution of the upper chord to the bending capacity was considered in the AZMI model.

Abduljabbar et al. [18] adopted two forms of steel truss-concrete composite beams, namely steel bar and double Angle steel bar, and conducted a monotone loading test study on them. The results show that the ultimate strength of the double-angle steel bar composite truss beam is 1.8-14% higher than that of the round steel bar composite truss beam, and no yield phenomenon occurs when the ultimate strength is reached. A reduction in the height of the steel truss will reduce the overall flexural stiffness, resulting in an increase in deflection.

In 1994, Lauer[19] conducted an experimental study on the mechanical properties of 8 steel truss-concrete composite beams with different shear connection degrees, using 6 different types of shear joints (Angle steel, stud, riveting screws, etc.). Based on the AZMI bearing capacity calculation model, the theoretical values of 8 specimens, such as upper and lower chord internal forces, total shear capacity of bolts and ultimate flexural capacity of composite beams are derived, and the theoretical values are compared with the experimental values. The results show that the AZMI model can be used to calculate the ultimate bearing capacity of steel truss-concrete composite beams with insufficient shear connection.

In 2015, Aiman[27] conducted an experimental study on the mechanical properties of two kinds of

steel trusses and compacted sheet concrete composite floors using mastic welding and Hilit screws. It is found that the specimens welded between the compression steel plate and the upper chord of the steel truss have better overall composite properties and significantly higher bending ability, while the specimens using Hilit screws will slide between the concrete plate and the steel truss, and the bearing capacity is only 62.5% of that of the specimens using the cement welding method, resulting in failure of the shear connection.

Luo et al. [28] tested the mechanical properties of three steel truss-concrete composite beams in partial shear connection, full shear connection and over-shear connection in 2019, and the test results showed that the number of shear joints would affect the flexural properties of the composite beams. Compared with the test results of full shear connection and over-shear connection, it is found that the overall shear performance of composite beams is not significantly improved when the number of shear connections exceeds the critical value.

In 2020, de Seixas Leal et al. [29] conducted a push-out test on the steel truss-concrete composite floor with three different shear connectors, and compared the test results with the predicted data of the theoretical model of four different steel truss-composite floors. The test results show that the performance of the shear connector used in the study and the flexural bearing capacity of the proposed floor system have obtained good results. However, model 3 based on complete plasticity of cross section is not sufficient to provide reliable ultimate load prediction, and in all cases, the flexural load ratio estimated by test and analysis is below 1.0.

Abduljabbar et al. [31] studied the performance of steel truss-concrete composite beams under impact load by using drop hammer test. They selected parameters such as span depth ratio, drop height and weight change. The test results show that under impact load, when the span depth ratio of steel truss decreases, the deflection increases slightly at the fourth impact, but when the weight is halved, the deflection decreases by about 55% at the same impact. The maximum impact force will decrease with the decrease of span depth ratio. Reducing the falling weight reduces the impact force and reaction force.

II. Specimen design and test process

The test specimen is a 3:1 hollow steel truss composite floor with no upper chord, as shown in Figure 2.1. The size design of the lower steel structure is shown in Table 2.1, and the size design of the concrete slab is shown in Table 2.2

Table 2.1 Dimensions of lower steel truss

Length /mm	Lower chord H Steel section H_1 xB_1 x t_1 xt_{w1} /mm	Stiffening plate thickness /mm	Web cross section H_2 xB_2 x t_2 xt_{w2} /mm	Web height /mm	Distance between Web 1 /mm	Distance between Web 2 /mm	Top plate L_g xB_g x t_g /mm
2800	50 x50 x3 x 3	3	100 x50 x3 x 3	80	100	125	126 x50 x 3

Table 2.2 Dimensions of concrete slabs

Slab length mm	Slab width mm	Slab thickness mm	Transverse reinforcement	longitudinal reinforcement
2800	460	40	Φ4@50	Φ4@50

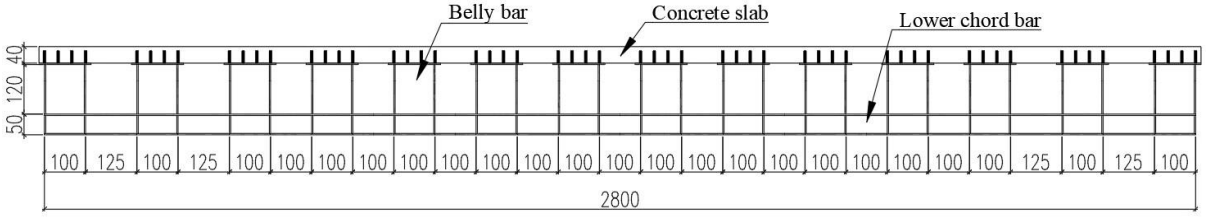

(a) Composite floor elevation plan

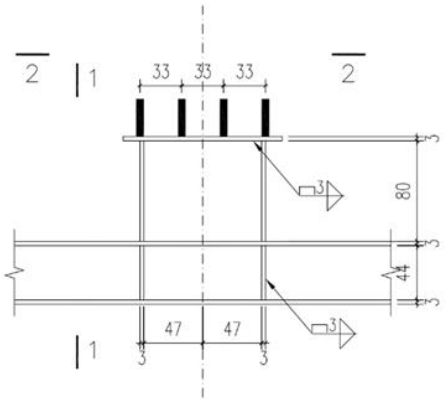

(b) Detailed drawing of nodes at the belly bar

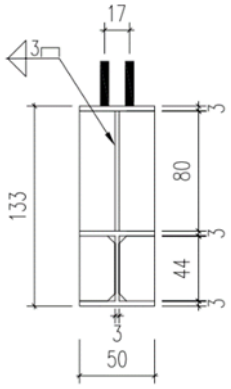

(c) 1-1 sectional details

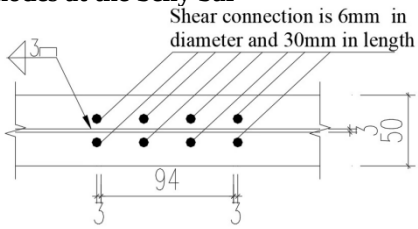

(c) Details of section 2-2

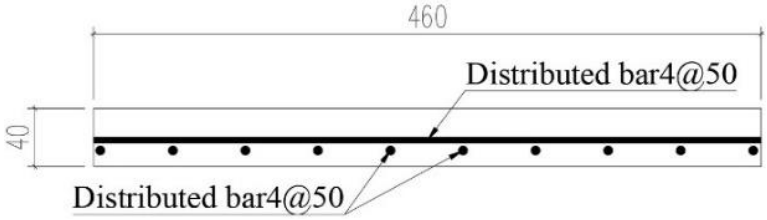

(d) Detailed drawing of reinforced concrete section reinforcement

Figure 2.1 Detailed design of steel truss and concrete slab

2.1 Steel property test

(1) Concrete:

The grouting material used in the concrete of this sample has many advantages such as artesiveness, self-densification, early high strength, micro-expansion, durability and environmental protection. The pouring is simple and the pouring quality is guaranteed. The concrete material property test adopts standard mold making and curing for 28 days under the same conditions as the specimen. The cube compressive strength test was carried out according to the standard test method provided by GB/T50448-2015, Technical Specifications for the Application of cement-based grouting Materials, as shown in FIG. 2.2 and FIG. 2.3. The test results are shown in Table 2.3.

According to the formula given in 4.0.2 of GB/T50152-2012, the axial compressive strength f0c, axial tensile strength f0t and elastic modulus E0c of concrete are calculated respectively, and the relevant calculation results are listed in Table 2.4.

Table 2.3 Test results of concrete properties

Sample number	instar	Measured compressive strength	Average compressive strength
C-1	28	75.02	
C-2	28	74.16	75.49
C-3	28	74.6	

Table 2.4 Test index of concrete material property

f^0_{cu}/Mpa	f^0_c/Mpa	f^0t/Mpa	E^0_c/N/mm^2
74.6	60.4	4.23	3.75×10^4

Figure 2.2 Production of standard specimen

FIG. 2.3 Compressive strength test of concrete

(2) Steel

The steel of this specimen is Q235B, which is made by cutting and welding, and the thickness of the component plate is 3mm. With reference to GB/T 228.1-2010 "Tensile Test Standard for Metal Materials", the proportional sample was designed and made, as shown in FIG. 2.4 and 2.5, and the material property test was carried out by ANS universal material property testing machine, as shown in FIG. 2.6. The results of wood property tests are shown in Table 2.5.

Table 2.5 Test results of steel material properties

Sample number	Yield point f_y		Tensile strength f_u			elongationδ%	
	Experimental value N/mm^2	average value	Experimental value N/mm^2	average value	Yield over average	Experimental value	average value
S-1	352.2		486.4			35.42	
S-2	362.8	364.1	493.8	496.3	0.73	34.28	34.34
S-3	377.3		508.8			33.33	

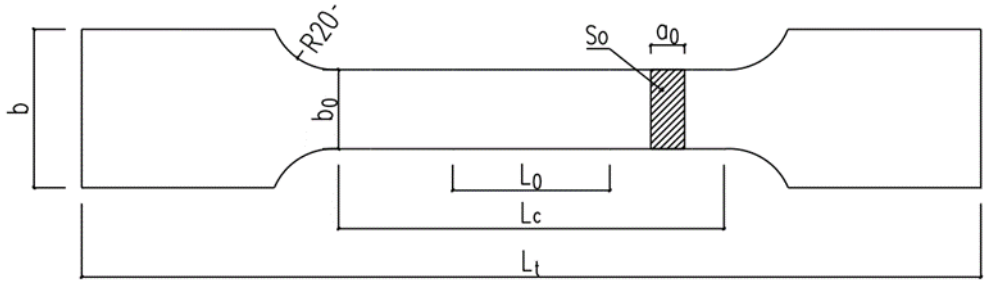

FIG. 2.4 Detail of steel sample

Figure 2.5 Steel proportion sample

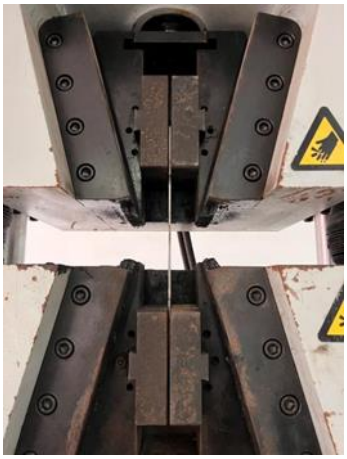

Figure 2.6 Steel properties test

2.2 Test scheme

In this experiment, 24 uniaxial strain measuring points and 6 strain flower measuring points were set up, and the concrete and steel compensating strain measuring points were set up. At the same time, 9 displacement measuring points were set up in this specimen, and a total of 53 channels were used.

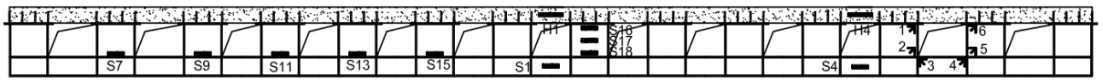

FIG. 2.7 Elevation of measuring point layout

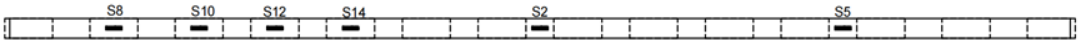

Figure 2.8 Lower chord flange measuring point arrangement (looking up)

FIG. 2.9 Arrangement of measuring points on the upper flange of the lower chord (overlooking)

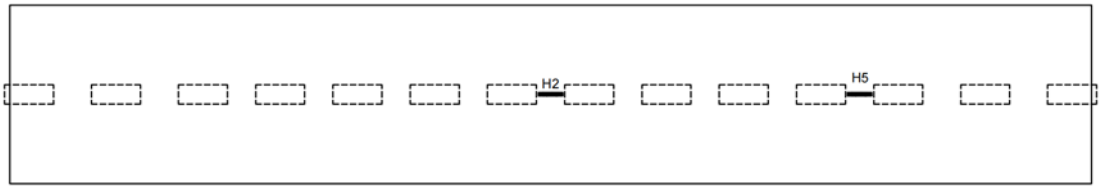

FIG. 2.10 Arrangement of measuring points on top of concrete slab

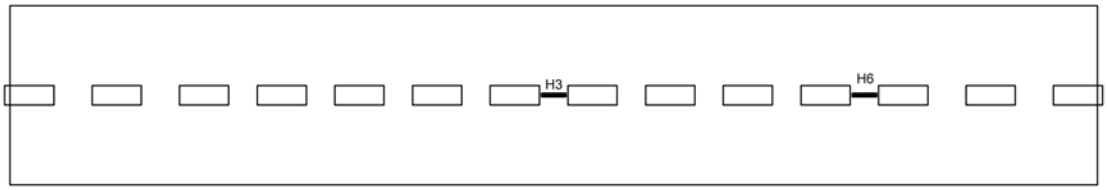

FIG. 2.11 Measuring point arrangement of concrete slab bottom

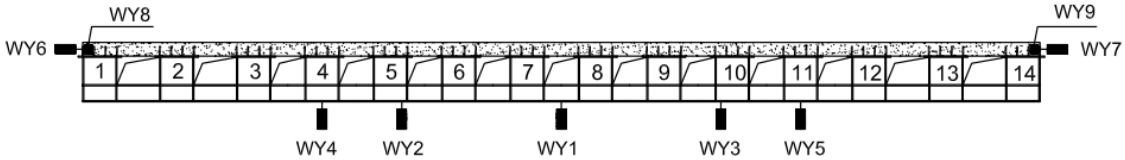

FIG. 2.12 Numbering of the belly rod and arrangement of displacement measuring points

2.3 Test process

This test can be divided into test preparation stage, pre-loading stage and formal loading stage. Each stage has a different degree of influence on the test results.

2.3.1 Test preparation stage

In the test preparation stage, the work mainly includes polishing the test point position of the specimen, meshing the upper and lower panels of the concrete, pasting the strain gauge and installing the displacement meter, connecting it to the signal acquisition system, and debugging the signal acquisition system until it can work

normally.

2.3.2 Preload phase

In this test, pre-load test will be carried out before the formal test loading to check whether the signal acquisition system and strain gauge displacement meter can work normally. In this test, two load levels were adopted for preloading, the first stage was loaded to 5kN, and the second stage was loaded to 10kN. In the preloading stage, the data of the signal acquisition system and each measurement point were stable, and each channel could work normally, which excluded the possible adverse effects for the formal test.

2.3.3 Formal Loading Phase

The test was divided into 17 loading stages, of which 0kN to 50kN were divided into 10 loading levels, and the subsequent loading levels were divided into seven levels according to the test conditions. The loading was controlled by displacement until the specimen was damaged. The formal loading stage can be divided into four stages: elastic development stage, elastoplastic development stage, failure stage and unloading stage according to the load-deflection relationship of unwinded hollow steel truss composite floor. The load-mid-span deflection relationship of the specimen is shown in Figure 2.13.

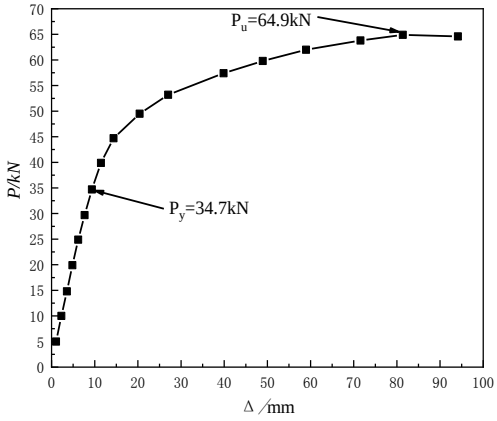

FIG. 2.13 load-mid-span deflection relationship

Elastic stage: In the early stage of loading, the specimen showed a large stiffness, and the relationship between the overall deflection of the specimen and the load was linear. In the process of load grade from the first load (5kN) to the sixth load (30kN), the overall stiffness of the specimen did not decrease, and the concrete slab did not crack. When the load grade reaches the seventh grade (34.7kN), cracks No. 1-8 appear near the loading point on the bottom of the concrete slab, but the cracks are too small in width and short in length (no more than 100mm), as shown in FIG. 2.14 and FIG. 2.15. Different from the area near the left and right equinox, there is no obvious crack in the middle span area of the concrete slab, as shown in Figure 2.16.

Elastoplastic stage: After loading grade 8 (39.9kN), cracks 9-11 were added to the bottom of the concrete slab near the left loading point, and cracks also appeared in the remaining areas. In addition, when the load reaches 40kN, the stiffness of the specimen decreases, and the specimen begins to enter the stage of elastic-plastic development. After loading to the ninth level load (44.7kN), cracks appear on the top of the concrete slab at the fixed hinge support, as shown in Figure 2.17. The cracks that originally appeared also developed rapidly, such as crack No. 4, which developed to the middle of the bottom of the concrete slab, as shown in Figure 2.18. When the load grade reaches grade 10, many cracks develop to the side of the slab, as shown in Figure 2.33. Cracks also appear on the top of the concrete slab on the right side (crack No. 25), as shown in Figure 2.19, some cracks run through to the other side (with the chord as the axis), and the mid-span deflection is 24.1mm. After entering the nonlinear development stage, the deflection increases rapidly and the cracks at the bottom of the plate develop rapidly. After the load value is loaded to 49.5kN, this phenomenon is more obvious. After the jack loading, the load value is not stable and decreases to a certain extent. Therefore, after the tenth grade load, the test adopts displacement control loading. It is worth noting that in the elastoplastic stage, when the load grade reaches 12 (57.4kN), the concrete slab bottom between the No.2 and No. 3 belly rods is stripped, as shown in FIG. 2.20. At this time, it is observed through the signal acquisition system that the steel lower chord rod in the mid-span section has entered the yield state in all sections. However, the lower chord web enters the yield state earlier than the lower flange of the lower chord in the right curved shear section. After reaching the load of 13 degrees (59.8kN), the cracks in the bottom of the concrete slab are densely distributed in the pure bending section and the bending shear section, but the cracks in the left bending shear section are significantly more than those on the right.

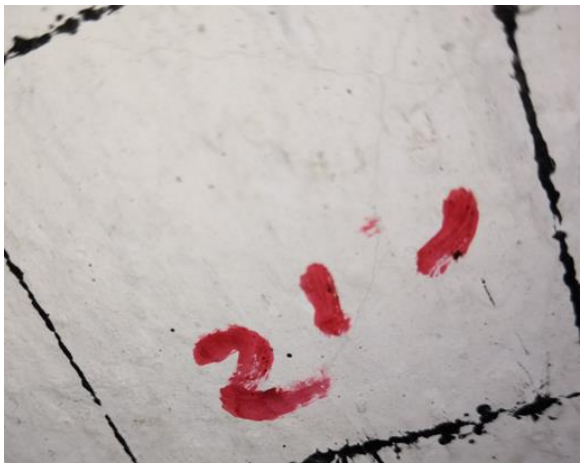

Figure 2.14 Crack No. 2 (Grade 7)

Figure 2.15 Cracks No. 4, 5 and 7 (Grade 7)

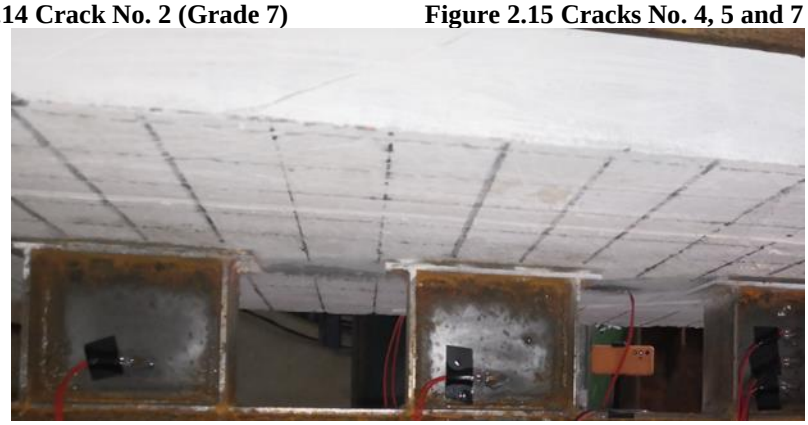

Figure 2.16 Mid-span concrete slab bottom (Grade 7)

Figure 2.17 Crack on the top of the concrete slab at the left end (Grade 9)

Figure 2.18 Fracture 4 developing to the middle (Grade 9)

Figure 2.19 Top crack of concrete slab at right end (Grade 10)

FIG. 2.20 Peeling of concrete slab bottom

Failure stage: After loading to grade 15 load, the overall deformation of the specimen has been serious. As shown in FIG. 2.21, the bending and shearing section of the lower chord has a torsional deformation at the connection between the abdominal rod and the chord rod, and the overall deformation of the specimen presents a "trapezoid" shape. Cracks along the beam length appeared at the top of the concrete slab at the right end, as shown in FIG. 2.22. Cracks developed rapidly at the bottom of the concrete slab at the lower part of the loading point on the left side. The width of the No. 26 main crack expanded continuously, and the neutral axis of the mid-span section was raised to the middle axis of the concrete slab, so many cracks developed to the upper side of the neutral axis. Therefore, it is considered that the specimen begins to enter the failure stage at this time. In the failure stage, the instability of the loading value of the jack is more serious, and the load value will fall back after each loading. In the process of loading from grade 15 to Grade 16 (64.9kN), there is a continuous sound. After the loading, it is found that the splicing place on the right chord of the left No. 3 belly rod is cracked and the fracture is even. At the same time, the bottom of the concrete slab on the right side also showed peeling phenomenon, and the left side was seriously peeling, and there was peeling between the No. 3 and No. 4 belly rods. The cracks became wider and some cracks, such as No. 26 cracks, ran through the bottom of the slab. At this time, the mid-span deflection reaches 81.38mm, reaching 1/34 of the span. In the process of loading to 17 load levels, the chord fracture expanded rapidly. In view of safety considerations, the loading was stopped, and the specimen was considered to have been damaged. At this time, the load value was 64.6kN, and after a period of time the load dropped to 62.8kN. At this time, the specimen was seriously damaged, the deflection increased to 94.13mm, the longitudinal crack through the top of the plate appeared, the crack width of the bottom of the plate increased to 0.66mm, for example, the crack of No. 26 increased to 0.66mm, the peel of the concrete slab became more serious, the opening at the chord fracture expanded to 2.5mm, and the weld was torn. The development of grade 16 to 17 specimens is shown in Figure 2.23-2.30.

FIG. 2.21 Overall deformation of the specimen (Grade 15)

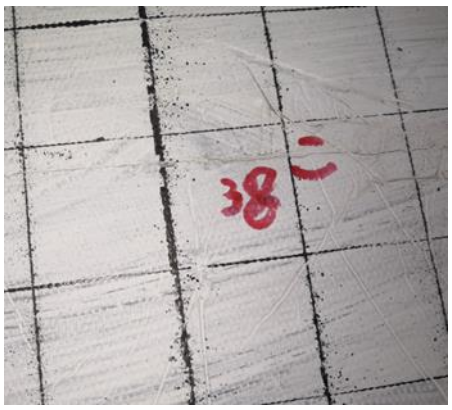

Figure 2.22 Longitudinal cracks on top of concrete slab (Grade 15)

Figure 2.23 Peeling of concrete (Grade 16)

Figure 2.24 Chord fracture (side view)

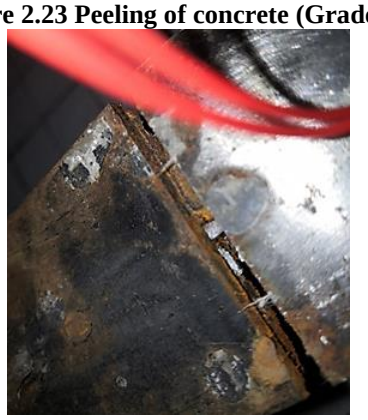

Figure 2.25 Chord fracture (looking up)

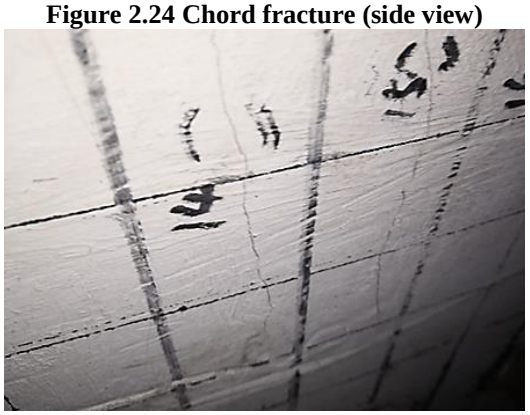

Figure 2.26 Fracture development (Grade 16)

FIG. 2.27 Serious peeling of concrete slab bottom (Grade 17)

FIG. 2.28 Expansion and severe deformation of chord fracture (Grade 17)

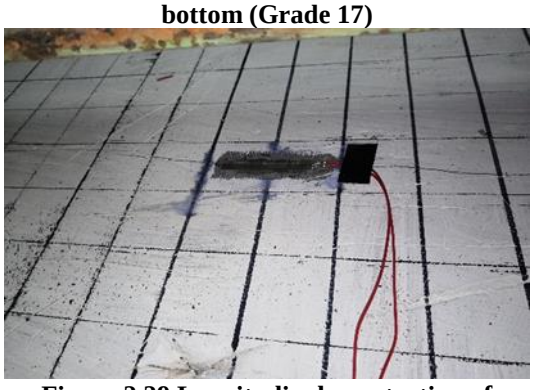

Figure 2.29 Longitudinal penetration of cracks in the top of concrete slab

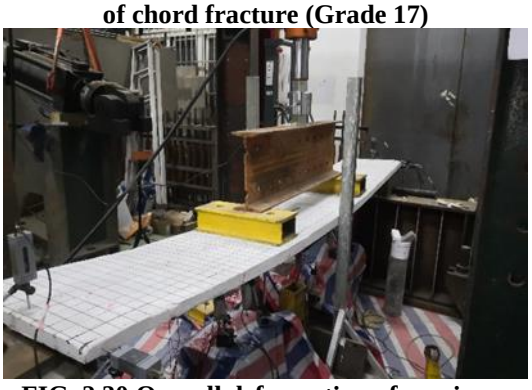

FIG. 2.30 Overall deformation of specimen (grade 17)

Unloading stage: After loading to grade 17 load, due to the serious damage of the specimen, the specimen is no longer loaded, and unloading is selected to end the test. The deflection of the specimen has a certain amount of retraction in the unloading stage, but the overall residual deflection still reaches 75.1mm. It is worth noting that the interface slip between the concrete slab and the steel beam was not observed during the

whole test, and the working performance of the stud connector was good. Figure 2.30-2.33 shows the damage state of the specimen after uninstallation (taken after the specimen is turned over).

Figure 2.30 Peeling place of the left bending shear section of the bottom of the concrete slab (inverted)

Figure 2.31 Fracture of the lower chord (inverted)

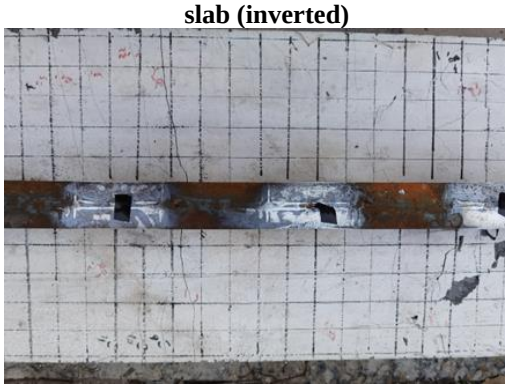

Figure 2.32 Main crack No. 26 (inverted)

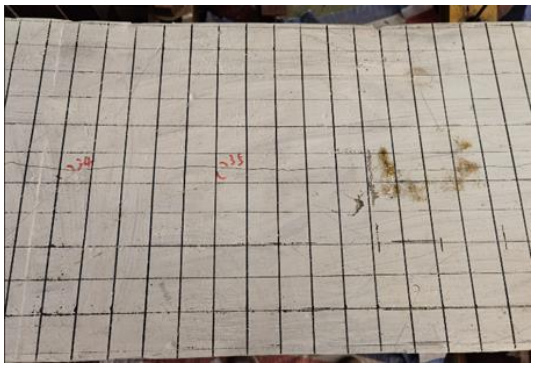

FIG. 2.33 Cracks in the top of the plate along the long direction of the beam

III. Analysis of test results

3.1 Flexural deformation analysis

(1) load-mid-span deflection analysis

It can be seen from the test phenomenon that the composite floor without upper chord steel truss maintains a good bearing capacity in the test, and the concrete slab and steel truss work well together without interface slip. And the composite floor has very good ductility, after the lower chord enters the yield, the deflection will be fully developed with the increase of load, and there will be no brittle failure phenomenon. According to the development of specimen deflection, the development of specimen deflection can be divided into elastic stage, elastoplastic stage and failure stage.

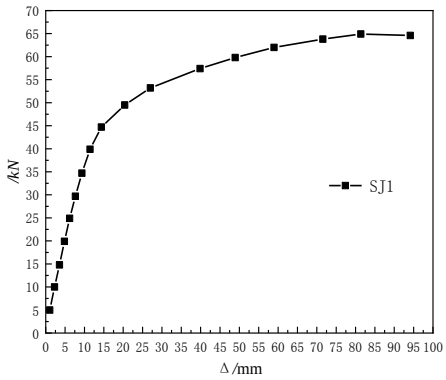

Figure 3.1 load-mid-span deflection relationship

Elastic stage: In the elastic stage, the lower chord of unwinded hollow steel truss composite floor is mainly subjected to tension, and the concrete slab is subjected to pressure, and their respective strains are small. The neutral axis of the specimen's hollow section is near the bottom of the concrete slab. The deflection of the specimen developed approximately linearly, and the stiffness of the specimen decreased slightly with the increase of load, but there was no significant stiffness degradation. After SJ1 was loaded to 34.7kN under the test load, cracks began to appear at the bottom of the concrete slab, mainly near the left loading point, and the main cracks of the later test specimen were also located in this area.

Elastoplastic stage: In the elastoplastic stage, the slope of load-mid-span deflection curve at this stage decreases with the increase of load, showing a curve form relationship. Compared with the elastic stage, the stiffness of SJ1 decreases significantly and the deflection increases continuously. The full section of the middle span of the lower chord rod enters the yield stage, the cracks of the concrete slab develop to the side of the slab and extend to the top of the slab, and the neutral axis of the specimen is gradually lifted upward.

Damage stage: In the process of loading the test load grade from 16 to 17, the deflection of SJ1 rapidly increased from 81.4mm to 94.13mm, while the load decreased from 64.9kN to 64.6kN. During this period, the bottom of the concrete slab appeared serious peeling phenomenon, the chord fracture expanded, the crack at the bottom of the slab developed to the top of the concrete slab, and the concrete slab withdrew from work. Stop loading for safety reasons. The real deflections of the specimen at the three stages are shown in Figure 3.2-3.4.

Figure 3.2 Elastic stage

Figure 3.3 Elastoplastic stage

Figure 3.4 Failure phase

(2) Overall deformation analysis

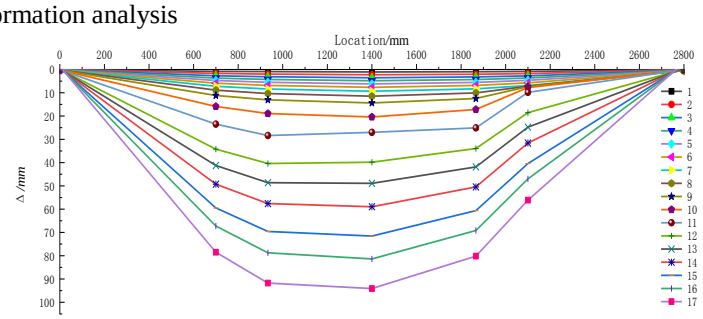

FIG. 3.5 Overall deformation of the specimen

FIG. 3.5 shows the overall deformation of the composite floor under different load grades. The deflection of the composite floor is not completely symmetrical, and the loading point in the test preparation stage is not completely symmetrical, which is the main reason for this phenomenon. Based on the analysis of the above phenomena, it can be seen that the hollow composite floor without upper chord steel truss has good mechanical performance, and the concrete slab and steel truss can achieve considerable cooperative work through the shear connection of pegs. The mid-span deflection of the specimen at the end of the elastic stage is 9.35mm, and the mid-span deflection at failure is 94.13mm, and the ductility coefficient is greater than 10, indicating that this type of composite floor has good ductility, and the overall deformation is large before failure, which can give users sufficient early warning. In addition, the specimen was twisted during the loading process, which was caused by some installation errors in the preparation stage of the specimen.

3.2 Stress-strain analysis

(1) Stress and strain analysis of the belly bar and lower chord of the left bending shear section

The left flexural shear section refers to the area between the fixed hinge support and the left three-point point, that is, the left loading point. This section analyzes the stress and strain of the belly bar and chord bar located in the left flexural shear section according to the measured test data.

FIG. 3.6 shows the load-stress diagram of the measuring point at the bottom of the belly bar of the left curved shear section. It can be seen from the load-stress diagram that the belly bar of the left curved shear section does not enter the yield stage in the span direction before the 16th load. FIG. 3.7 shows the load-stress diagram of the lower flange measuring points of the lower chord of the above four belly rods. Compared with the load grade of the measuring points at different positions when they enter the yield stage, it can be seen that the closer to the loading point, the earlier the yield time of the lower flange. The lower flange of measuring point No. 5 exceeds the ultimate strength of steel 496.3MPa after the tenth grade load, and enters the strengthening stage. The curve recurred after grade 17 load, which was caused by the fracture of the right chord of measuring point No. 3, which resulted in the redistribution of stress inside the steel truss.

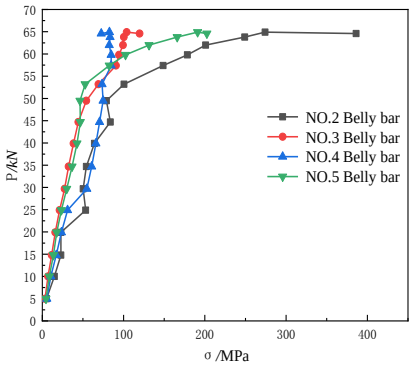

FIG. 3.6 Load-stress relationship of the belly bar in left flexural shear section

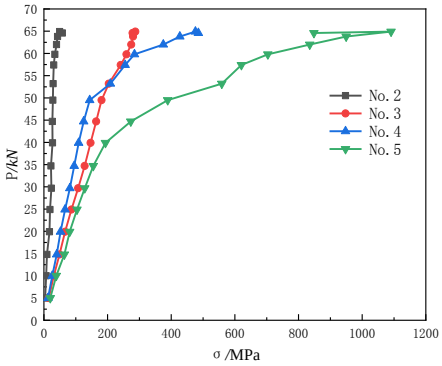

Figure 3.7 Load-stress relationship of the left bending shear section corresponding to the lower flange of the chord

FIG. 3.8 and FIG. 3.9 respectively compare the load-strain relationship between the lower measuring point of the No. 2 and No. 5 belly bar and the lower flange of the lower chord bar in the same section. By observing the two figures, it can be found that the strain generated at the lower part of the belly bar in the same section is much lower than the strain at the lower flange of the chord bar in the same section. FIG. 3.10 shows the strain comparison between No. 6 belly bar in the pure bend section and that in the flexural shear section at the same height measurement point. It can be found that the strain at the bottom of No. 6 belly bar on the right side of the left tripoint is negative, indicating that compressive strain is generated there, which is completely different from the strain stress distribution of the belly bar in the flexural shear section.

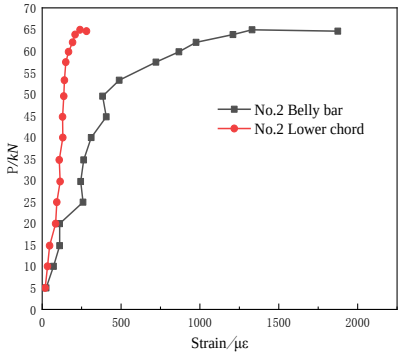

FIG. 3.8 No. 2 belly rod and flange strain under the same section

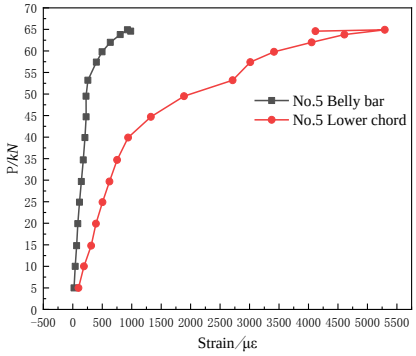

FIG. 3.9 Strain of No. 5 belly rod and flange under the same section

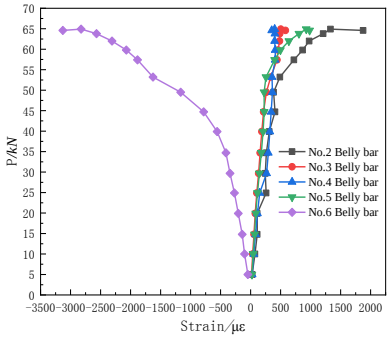

FIG. 3.10 Comparison of load-strain relationship between the abdomen bar of pure bending section and the left bending shear section

(2) Fasting section stress-strain analysis

FIG. 3.11 and FIG. 3.12 respectively show the strain and stress distribution of the empty cross section in the middle span, and FIG. 3.13 and FIG. 3.14 show the strain and stress distribution of the right cross section respectively. The positions in the figure represent the vertical distance between the measuring point and the bottom of the cross section, where the distance 133-173 represents the range of the concrete slab, and the distance 0-50 represents the range of the lower chord. It can be seen that in the elastic stage, the hollow section of the middle span is geometrically discontinuous. Considering that the lower chord mainly relies on the upper and lower flange to bear the tension, the strain stress of the upper and lower flange of the chord is larger than that of the web. If the strain of the web is ignored, the strain of the middle span section presents a linear distribution along the height of the section, with obvious rules, and has some characteristics assumed by the normal section. On the other hand, the strain distribution of the right flexural shear section is still approximately linear at the front of the fourth grade load, and the distribution is broken after the fourth grade load. In addition, at the initial stage of loading, the neutral axis of both sections is located at 3-4mm above the bottom of the concrete slab, so it can be determined that the neutral axis of the hollow section is located in the concrete slab. When the load is loaded to the sixth level, it can be found that the neutral axis is lifted. By observing the stress distribution along the height of the two sections, it is found that the stress at the bottom of the two sections of the concrete slab is positive, indicating that the concrete slab is strained from the beginning of the test, while the stress in the top of the concrete slab and in the slab is mostly negative, indicating that the area is under pressure. It further indicates that the neutral axis at the hollow section of the middle span is located in the concrete slab.

FIG. 3.15 shows the distribution of stress in the mid-span section of the chord and the stress in the right flexural shear section along the height under the nine-order load. At this time, the lower flange of the mid-span chord has entered the tension yield state, but the web and upper flange still maintain elasticity, while the whole section of the right flexural shear section is in the elastic stage. The tension stress of the web in mid-span section is less than that of the upper and lower flange, indicating that the upper and lower flange of H-beam chord is the main tension position. Figure 3.16 shows the stress distribution of No. 8 belly bar along the height. According to the analysis of the figure, it can be seen that the belly bar of the pure bending section is in an elastic state during most stages of the whole test, and contributes little to the overall flexural bearing capacity of the composite truss, and its main function is to connect the concrete slab to the chord bar.

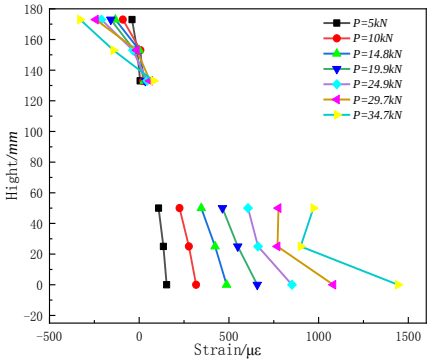

FIG. 3.11 Strain distribution at mid-span fasting cross section

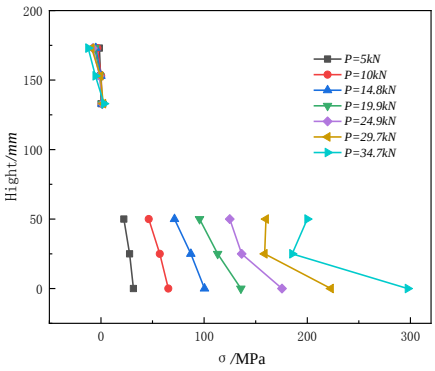

FIG. 3.12 Stress distribution of mid-span hollow cross section

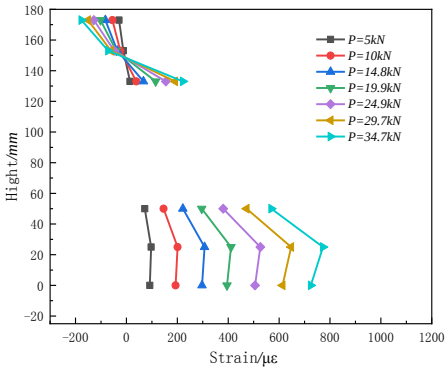

FIG. 3.13 Strain distribution at the right fasting section

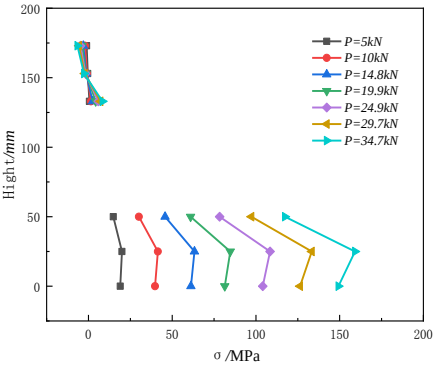

FIG. 3.14 Stress distribution of the right hollow section

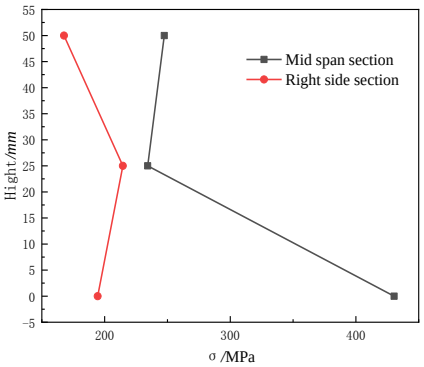

FIG. 3.15 Comparison of stress distribution in lower chord section

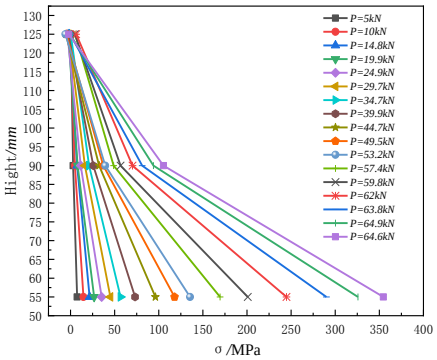

FIG. 3.16 Stress distribution of No. 8 belly bar

（3）Analysis of stress distribution around hole

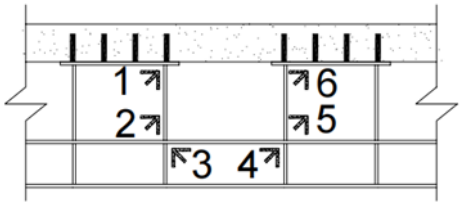

FIG. 3.17 Distribution of measuring points around holes

Due to the unique structure of the opening of the composite floor without upper chord, the surrounding stress distribution is also relatively complex, and stress concentration is more likely to occur near the opening of the flexural shear section. In order to explore the stress distribution rule, strain flowers are arranged around the second opening of the flexural shear section in this specimen, and their specific positions are shown in Figure

3.17. FIG. 3.18 and 3.19 show the comparison between the maximum and minimum principal stresses of the six measuring points around the orifge under grade 6 load and Grade 12 load respectively.

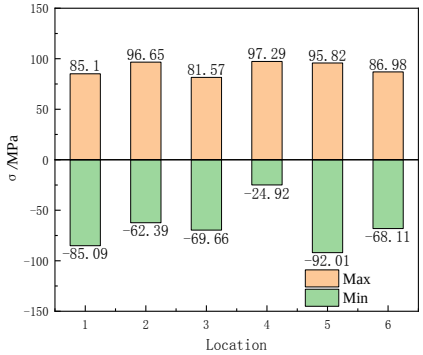

FIG. 3.18 Nominal stress distribution around holes (Level 6)

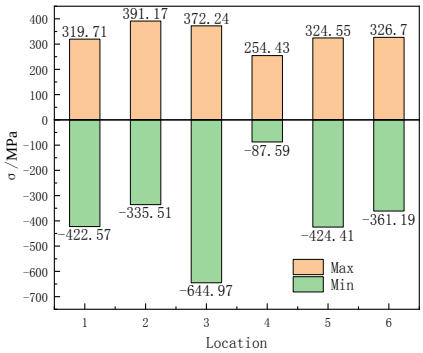

FIG. 3.19 Nominal stress distribution around hole (12th order)

In the elastic stage, the maximum principal stress distribution is relatively uniform, and the tensile stress of No. 1 and No. 6, No. 2 and No. 5 measuring points on the two ventral rods is approximately equal. Different from the maximum principal stress, the distribution of the minimum principal stress is relatively discrete, the maximum occurs at measuring point No. 5, and the minimum is at measuring point No.4. The minimum principal stress at measuring point No. 5 located on the lower left side of the belly bar is 1.47 times that of the principal stress at measuring point No. 2 located on the lower right side of the belly bar. The maximum principal stress and minimum principal stress at measuring points No. 2 and No. 6 are roughly the same at the sixth level load, and the same phenomenon is also reflected in the measured results at measuring points No. 1 and No. 5.

3.3 Failure mode and fracture development analysis

The bearing capacity of this specimen reached the highest value at the 16th load. At this time, the lower flange of the right side of the No. 3 belly bar in the left flexural shear section of the composite floor chord rod broke, and the concrete peel occurred in the left and right flexural shear section of the bottom of the concrete slab, and the left side was more serious. During the loading process of level 16 to 17, the deflection increased rapidly and the fracture of the original chord continued to expand until the composite floor experienced a "bang" sound before the loading stopped. At this time, the composite floor was seriously damaged, cracks appeared on the top of the concrete slab along the long direction of the beam nearly throughout the whole span, and the bottom of the concrete slab was seriously peeled off (FIG. 3.20). A peel joint with a width of 10-15mm appeared, and the chord also showed a large deformation. The crack at the fracture expanded to 2.5mm (FIG. 3.21), and the load dropped to 62.6kN after stopping the loading. Therefore, it was considered that the specimen had reached the state of failure.

In the initial stage of loading, the principal tensile stress at the edge of the section under the section is horizontal, and a short vertical crack will be formed. With the increase of load, the bending shear crack of the simple supported concrete beam will gradually develop towards the loading point. The characteristics of the bending shear crack are wide at the bottom and thin at the top. The reason for the formation of peel cracks in SJ1 is similar, but the difference is that the width of the concrete slab of the composite floor is larger. Due to the influence of the shear lag effect of the composite beam, the normal stress on the outside of the connection between the abdominal bar and the concrete slab is higher than that on the outside wing edge, and the cracks are generated there. Secondly, because the connection between the steel truss and the concrete slab is not continuous, most of the shear force of the composite floor is borne by the belly bar, and there will be a large stress concentration phenomenon at the joint of the belly bar and the concrete slab. Therefore, cracks will gradually develop to the connection area between the adjacent belly bar and the concrete slab with the increase of load, and the longitudinal cracks of the lower part are wider and the upper part is finer when the failure occurs. The transverse fracture is "wide in the middle and thin at both ends", and the whole fracture is "triangle-like". The string fracture may be a phenomenon caused by the machining error of the string.

In this test, steel pad blocks are arranged above the loading point, and the concentrated load is imposed on the left and right pad blocks through the distribution beam, which will gradually decrease the load from the width of 1/2 plate (that is, the distribution area of steel truss) to the edge of the concrete slab under the pad block, so a large bending moment will be formed at the width of 1/2 plate. After the truss enters the failure stage, The

top of the concrete plate under the pad has a crack along the beam length at 1/2 of the width of the plate. When failure occurs, the cracks under the left and right loading points are connected along the long direction of the beam, forming cracks that almost run through the whole span.

Fig. 3.20 Peeling of concrete slab bottom

Fig. 3.21Lower chord fracture

FIG. 2.72 and 2.73 show the crack distribution of the top and bottom of the specimen after loading. It can be seen that the cracks at both ends of the top of the plate are distributed near the No. 1 and No. 14 belly rods, and the longitudinal penetrating cracks basically develop along the steel truss area. The cracks in the pure bend section are relatively fine and mostly surface cracks, which reflects excellent bending resistance. The main crack appears near the left loading point, which develops deeper and wider in the direction of plate thickness, which is one of the reasons for the failure of composite floor. The cracks in the left flexural shear section are closely related to the peeling phenomenon of the bottom of the concrete slab in this area. It can be seen that the main peeling cracks are located in the fasting range between the belly bar and the joint area between the belly bar and the concrete slab, indicating that the shear connection between the belly bar and the concrete slab is reliable, and this intermittent shear connection is also one of the reasons for the peeling of the bottom of the concrete slab.

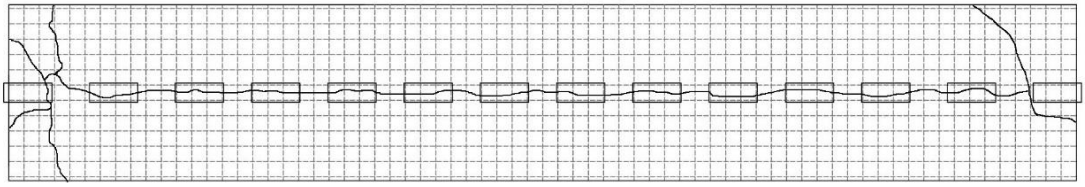

Figure 3.22 Crack distribution on top of concrete slab

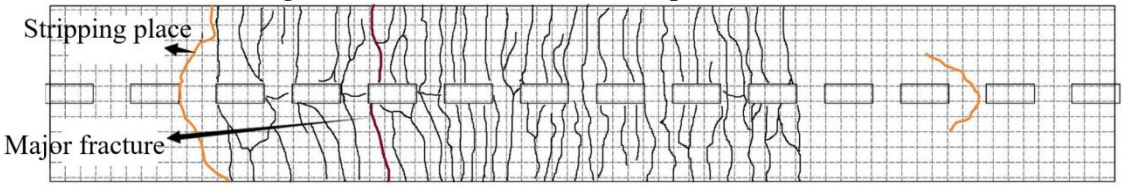

FIG. 3.23 Distribution of cracks at the bottom of concrete slab

IV. Conclusion

The hollow steel truss composite floor without upper chord is a new type of composite floor, and the upper chord and diagonal bar of the traditional steel truss composite beam are eliminated, which saves the building space. In this chapter, the purpose, scheme, process and results of static loading test of unwinded hollow steel truss composite floor are introduced in detail. It can provide a detailed reference for the subsequent test and design research of the structure.

According to the test phenomenon, the flexural deformation, stress strain, crack development and failure mode of the specimen are analyzed in this chapter. The following conclusions can be drawn:

(1) In the composite floor system without upper chord, the concrete slab and the lower steel truss are connected by pegs, maintaining excellent collaborative working ability.

(2) The composite floor has good ductility, and there will be a long elastoplastic development stage before failure, and there will be no brittle failure, which can give users enough safety warning.

(3) The development of composite floor is mainly divided into three stages: elastic, elastic-plastic and failure, with high bearing capacity. The increase of the number of belly rods can improve the bearing capacity of

composite floor.

(4) In the elastic stage, the fasting section strain of the mid-span and flexural shear section of the composite floor basically conforms to some characteristics assumed by the plain section. During the whole development stage of the structure, the neutral axis of the fasting section is always located inside the concrete slab and will gradually lift upward with the increase of load.

(5) Under the mode of two-point symmetric concentrated loading, the belly bar in the flexural shear section will assume the role of transferring shear force, while the belly bar in the pure flexural section area mainly connects the lower chord bar with the concrete slab.

(6) The cracks of composite floor in elastic stage and elastoplastic stage are mainly cracks at the bottom of concrete slab along the width direction. At the end of elastoplastic stage and failure stage, peel cracks will occur at the bottom of concrete slab in the hollow area near the support, and the cracks will start to develop diagonally from the belly bar near the middle span of the concrete slab, and the surrounding concrete will crumble during failure. In addition to the peeling cracks, cracks along the distribution area of the belly bar will appear when the concrete slab roof is damaged.

REFERENCES

[1]. Azmi M-K. Composite Open-Web Trusses with Metal Cellular Floor[D]. McMaster University, 1972.Hamilton

[2]. Abduljabbar M S, Hamood M J, Abdulsahib W S. Flexural behavior of composite open web steel joist and concrete slab[C]//IOP Conference Series: Materials Science and Engineering. IOP Publishing, 2020, 737(1): 12-17.

[3]. Lauer D-F. Ultimate strength analysis of composite and fully composite open - web steel joists[D]. Virginia, Virginia Polytechnic Institute and State University, 1994.

[4]. Aiman M. Behaviour of Open Web Steel Joist in Composite Deck Floor System[D]. Ontario,University of Windsor, 2015.

[5]. Aiman M. Behaviour of Open Web Steel Joist in Composite Deck Floor System[D]. Ontario,University of Windsor, 2015.

[6]. deSeixas leal L,de Miranda batista E. Experimental investigation of composite floor system with thin-walled steel trussed beams and partially prefabricated concrete slab[J]. Journal of Constructional Steel Research, 2020, 172: 1-18.

[7]. Abduljabbar M-S,Hamood M-J,Abdulsahib W-S. Behavior of Composite Open Web Steel Joist under Impact Loading[J]. Journal of Engineering Science and Technology, 2020, 5(15): 3314-3333.